

Moments of structure functions for $N_f = 2$ near the physical point

G. S. Bali, S. Collins*, B. Gläbke, M. Göckeler, J. Najjar, R. Rödl, A. Schäfer, R. Schiel, A. Sternbeck, W. Söldner

Institut für Theoretische Physik, Universität Regensburg, 93040 Regensburg, Germany

E-mail: sara.collins@physik.uni-regensburg.de

We report on our on-going study of the lower moments of iso-vector polarised and unpolarised structure functions, g_A and $\langle x \rangle_{u-d}$, respectively, and the iso-vector scalar and tensor charge, for $N_f = 2$ non-perturbatively improved clover fermions. With pion masses which go down to about 150 MeV, we investigate finite volume effects and excited state contributions.

31st International Symposium on Lattice Field Theory - LATTICE 2013

July 29 - August 3, 2013

Mainz, Germany

*Speaker.

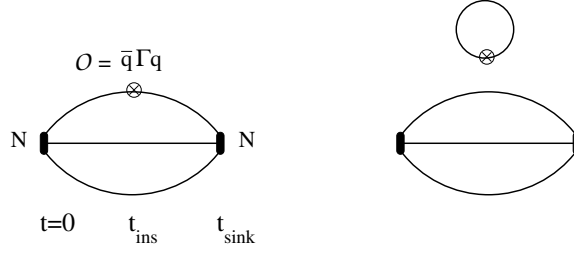


Figure 1: The connected (left) and disconnected (right) contributions to nucleon three-point functions for a nucleon source at $t = 0$, sink at t_{sink} and operator insertion at t_{ins} .

1. Introduction

In recent years it has become clear that g_A and $\langle x \rangle_{u-d}$, benchmark quantities for lattice calculations of nucleon structure, are sensitive to a number of sources of systematic error - finite volume, non-physical pion mass, excited state contamination and finite lattice spacing. Continuing improvements in computing power, algorithms and analysis techniques mean systematics can now be investigated and in some cases removed.

In the following we present preliminary results for these quantities along with the iso-vector scalar and tensor charges, g_S and g_T , respectively, for $N_f = 2$ ensembles including different lattice spacings, pion masses and volumes focusing on studying excited state effects. The iso-vector combination only requires the calculation of the connected quark diagram, see Figure 1. We have also determined the disconnected contributions to the scalar matrix element. This and the iso-vector generalised form factors for a range of operators are detailed in [1]. While many lattice simulations now include dynamical strange quarks, so far the strange quark has been found to play a minor role in nucleon structure and $N_f = 2$ simulations are still relevant.

2. Simulation details

The results were computed using ensembles generated by QCDSF and the Regensburg Group, with $N_f = 2$ degenerate flavours of dynamical sea quarks using the non-perturbatively improved clover action at two lattice spacings and a range of pion masses from $m_\pi \sim 490 - 150$ MeV, see Table 1. Two volumes are available for two values of m_π , in particular at the near physical point.

The two-point and three-point functions were computed using Wuppertal smeared sources and sinks with APE smeared gauge links. For each ensemble the smearing was optimised to minimize the excited state contributions to the nucleon two-point function. The connected three-point functions were generated using the standard sequential propagator method which involves fixing the sink timeslice (t_{sink}). An alternative approach using stochastic estimates has been investigated, see [2]. The values of t_{sink} were chosen using ensemble II. For $t_{\text{sink}} = 15a \sim 1$ fm on this ensemble no significant excited state contributions to the quantities $\langle x \rangle_{u-d}$ and g_A were found. This was checked by performing an excited state analysis with multiple t_{sink} s, described in the next section. $t_{\text{sink}} = 15a$ was then used for all $\beta = 5.29$ ensembles and rescaled for $\beta = 5.40$. Multiple measure-

	β	κ	Volume	$N \times M$	$a/$ fm	$m_\pi/$ MeV	Lm_π	t_{sink}/a
I	5.29	0.13620	24×48	1124×2	0.07	430	3.7	15
II		0.13632	32×64	2027×2 (1)		294	3.4	(7,9,11),13,15,17
III		0.13632	40×64	2028×2		289	4.2	15
IV		0.13640	48×64	3400×2		157	2.7	15
V		0.13640	64×64	940×3		150	3.5	15
VI	5.40	0.13640	32×64	1170×2	0.06	491	4.8	17
VII		0.13660	48×64	2178×2		260	3.8	17

Table 1: Details of the ensembles used in our analysis including approximate lattice spacings and pion masses and the values of t_{sink} used for the sequential propagators. The number of configurations (N) and measurements made per configuration (M) are indicated. For $t_{\text{sink}}/a = 7, 9$ and 11, ensemble II, only one measurement per configuration is made.

ments were performed on each configuration. Autocorrelations were investigated by binning the data with different bin sizes.

In order to reduce the discretisation effects to $O(a^2)$, the operators, as well as the quark action, need to be (nonperturbatively) improved. The $O(a)$ improved renormalised operators have the form [3]

$$O^{\text{improv}} = Z_O [(1 + b_O a m_q) O + a c_O O']. \quad (2.1)$$

For g_A , $O = \bar{q} \gamma_\mu \gamma_5 q$, and the improvement term, $a c_O O' = a c_A \partial_\mu \bar{q} \gamma_5 q$, does not contribute for forward matrix elements. We use the Z_O factors determined non-perturbatively [4, 5] and the b_O factors from [6]. Setting $c_O = 0$, our values for g_A will have leading $O(a^2)$ effects, while $\langle x \rangle_{u-d}$, g_S and g_T have $O(a)$.

3. Excited state fits

Excited state contributions to nucleon structure have been investigated by a number of groups recently, see, for example, [7, 8, 9, 10, 11]. Our analysis on ensemble II is similar to that performed in reference [11]. We fitted the two-point (C_{2pt}) and three-point (C_{3pt}) functions at multiple t_{sink} s simultaneously using the functional forms:

$$C_{2pt}(t_{\text{sink}}) = \sum_{\vec{x}} \langle \mathcal{N}(\vec{x}, t_{\text{sink}}) \overline{\mathcal{N}}(\vec{0}, 0) \rangle = |Z_0|^2 e^{-m_0 t_{\text{sink}}} + |Z_1|^2 e^{-m_1 t_{\text{sink}}} + \dots \quad (3.1)$$

$$= e^{-m_0 t_{\text{sink}}} [|Z_0|^2 + |Z_1|^2 e^{-\Delta m t_{\text{sink}}} + \dots] \quad (3.2)$$

$$C_{3pt}(t_{\text{sink}}, t_{\text{ins}}) = \sum_{\vec{x}, \vec{y}} \langle \mathcal{N}(\vec{x}, t_{\text{sink}}) O(\vec{y}, t_{\text{ins}}) \overline{\mathcal{N}}(\vec{0}, 0) \rangle \quad (3.3)$$

$$= |Z_0|^2 \langle N_0 | O | N_0 \rangle e^{-m_0 t_{\text{sink}}} + Z_1^* Z_0 \langle N_1 | O | N_0 \rangle e^{-m_0 t_{\text{ins}}} e^{-m_1 (t_{\text{sink}} - t_{\text{ins}})} \\ + Z_0^* Z_1 \langle N_0 | O | N_1 \rangle e^{-m_1 t_{\text{ins}}} e^{-m_0 (t_{\text{sink}} - t_{\text{ins}})} + |Z_1|^2 \langle N_1 | O | N_1 \rangle e^{-m_1 t_{\text{sink}}} + \dots \quad (3.4)$$

$$= |Z_0|^2 e^{-m_0 t_{\text{sink}}} \left(B_0 + B_1 [e^{-\Delta m (t_{\text{sink}} - t_{\text{ins}})} + e^{-\Delta m t_{\text{ins}}}] + B_2 e^{-\Delta m t_{\text{sink}}} \right) + \dots \quad (3.5)$$

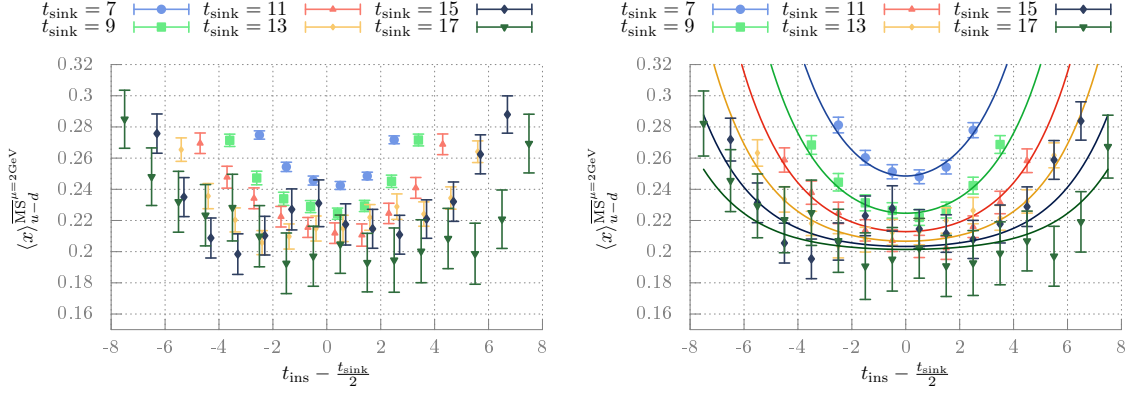


Figure 2: (Left) The raw ratio $(C_{3pt}/C_{2pt}) \cdot$ factor for ensemble II for different t_{sink} s, where the factor includes the renormalisation and improvement constants and mass term necessary to convert to $\langle x \rangle_{u-d}^{\overline{\text{MS}}}$ at $\mu = 2 \text{ GeV}$. (Right) The raw results for C_{3pt} , ensemble II, divided by the fit result for $|Z_0|^2 e^{-m_0 t_{\text{sink}}}$, compared to the corresponding fit function divided by the same quantity: $B_0 + B_1[e^{-\Delta m(t_{\text{sink}} - t_{\text{ins}})} + e^{-\Delta m t_{\text{ins}}}] + B_2 e^{-\Delta m t_{\text{sink}}}$. The same factor is included as for the figure on the left in order to convert to $\langle x \rangle_{u-d}^{\overline{\text{MS}}}$ at $\mu = 2 \text{ GeV}$.

where \mathcal{N} destroys the nucleon, O is the current insertion and $Z_i = \langle 0 | \mathcal{N} | N_i \rangle$. $|N_0\rangle$ and $|N_1\rangle$ represent the nucleon ground and first excited state, respectively. For the cases considered here, it is sufficient to consider zero initial and final momentum in order to extract forward matrix elements.

The matrix element of interest is given by $B_0 = \langle N_0 | O | N_0 \rangle$ while $B_1 \propto \langle N_1 | O | N_0 \rangle$ gives the transition matrix element from the ground to the first excited state and $B_2 \propto \langle N_1 | O | N_1 \rangle$ the first excited state matrix element. These fits can be compared to the traditional approach of fitting the ratio of three-point to two-point functions to a constant:

$$\frac{C_{3pt}(t_{\text{sink}}, t_{\text{ins}})}{C_{2pt}(t_{\text{sink}})} = B_0 + \dots \quad (3.6)$$

We illustrate the results for the example of $\langle x \rangle_{u-d}$, which we found to have significant excited state contributions at small t_{sink} . Figure 2 displays the raw results for the six t_{sink} values. Agreement is found for $t_{\text{sink}} \geq 11a$ for $t_{\text{ins}} - t_{\text{sink}}/2 \approx 0$. For $t_{\text{sink}} \geq 13a$, the plateau extends for several timeslices, however, as expected, the statistical errors also increase. Correlated fits to all three-point and two-point functions using Eqs. (3.2) and (3.5) (truncating after the first excited state) produced good $\chi^2/d.o.f \approx 1$ and were stable against changes in the fitting ranges to C_{3pt} and C_{2pt} . An example of one of the combined fits is shown in Figure 2. For the smearing we have used, the ground and first excited state are the dominant contributions for t_{sink} as small as $7a$. In Figure 3, a result of the combined fit is compared to the values obtained fitting the ratio C_{3pt}/C_{2pt} to a constant for different t_{sink} ; consistency is found between the two methods for $t_{\text{sink}} \geq 11a$. From this analysis we find our optimised smearing is sufficient to extract the ground state matrix element using a single $t_{\text{sink}} \geq 11a$ and we take the conservative choice of $15a$. We remark that with a less optimised smearing we found a $t_{\text{sink}} > 15a$ insufficient.

For the other ensembles, where we only have one t_{sink} , we check the size of the excited state contamination by performing fits using Eqs. 3.2 and 3.5 and the parameters proportional to the

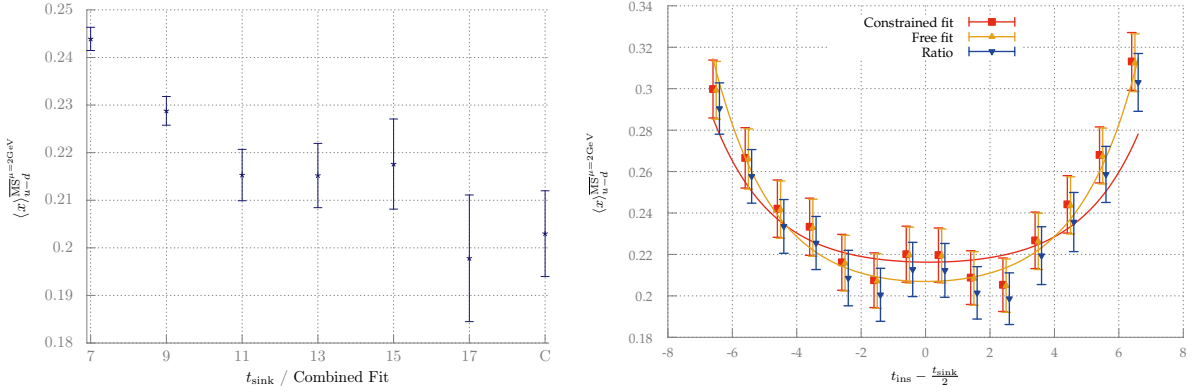


Figure 3: (Left) For ensemble II, $\langle x \rangle_{u-d}^{\overline{MS}^{\mu=2\text{GeV}}}$ extracted from constant fits to the ratio C_{3pt}/C_{2pt} (Eq. (3.6)) for different t_{sink} and extracted from the combined fit to C_{3pt} and C_{2pt} , for all t_{sink} s, including the first excited state, denoted by C . (Right) For ensemble IV, the raw ratio C_{3pt}/C_{2pt} factor is shown (red triangles). The two lines indicate fits (i) constraining the excited state parameters using the results from ensemble II (blue line) and (ii) leaving B_1 free and $B_2 = 0$ (green line). For each of these fits the raw results for C_{3pt} factor, divided by $|Z_0|^2 e^{-m_0 t_{\text{sink}}}$, is shown.

excited state matrix elements, B_1 and B_2 , extracted using ensemble II (which we assume to be slowly varying with the quark mass and lattice spacing). Figure 3 shows such a constrained fit for ensemble IV. The value extracted for the ground state is consistent with a fit using the same functional form, but with B_1 as a free parameter and $B_2 = 0$ ¹. It is also consistent with the result of a constant fit to C_{3pt}/C_{2pt} .

The excited state fitting analysis was similarly successful for the other quantities of interest. We note that for g_A , significant excited state contributions were found for $t_{\text{sink}} = 7$ and 9, however, these contributions cancelled in the ratio C_{3pt}/C_{2pt} , giving a plateau for the ratio, even for the smallest t_{sink} . For g_S , the ground state was dominant for all t_{sink} for the iso-vector combination in the ratio C_{3pt}/C_{2pt} . This appears to be due to a cancellation in the $u - d$ combination since for the iso-scalar matrix elements, not presented in this work, there were significant excited state contributions. The tensor charge analysis was similar to that for $\langle x \rangle_{u-d}$.

4. Results

In the following we present results obtained from a constant fit to the ratio C_{3pt}/C_{2pt} , for a single t_{sink} . Figure 4 shows our results for g_A , $\langle x \rangle_{u-d}$, g_T and g_S from all ensembles as a function of m_π^2 . Recent work from other groups is indicated, where for g_A and $\langle x \rangle_{u-d}$, due to the large number of previous determinations, we only compare with other $N_f = 2$ calculations. Recent $N_f = 2 + 1$ and $2 + 1 + 1$ results are reviewed in [12]. For the scalar and tensor charge most other results are for $N_f = 2 + 1$ and $2 + 1 + 1$.

¹This parameter cannot be determined from fits to a single t_{sink} .

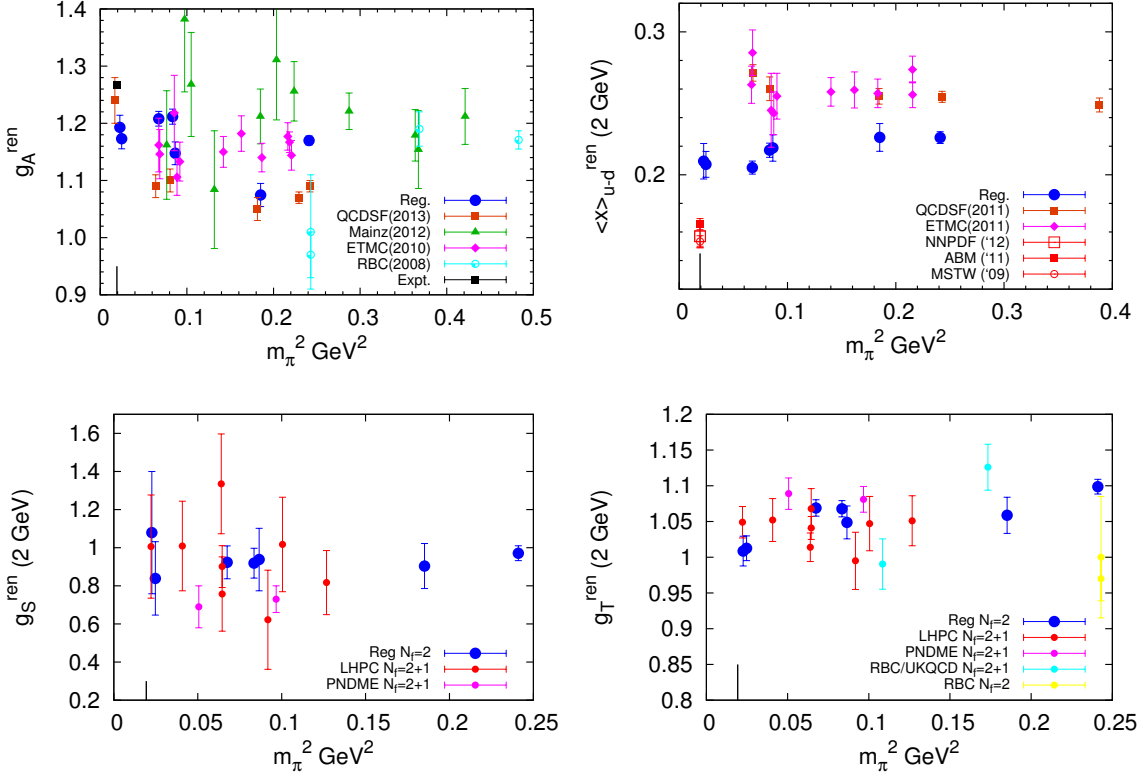


Figure 4: Results obtained from all ensembles as a function of m_π^2 (blue circles) compared to previous works. The physical point is indicated by a vertical line. For g_A and $\langle x \rangle_{u-d}$ only $N_f = 2$ determinations are shown. For the former, the experimental result is shown as a black square, while for the latter, the expectations from PDF parameterisations of the NNPDF, ABM and MSTW groups are shown.

Considering g_A first, one can see in Figure 4 that there is a significant dependence of our results on the volume and possibly m_π and a . Consistency is found with the values from the Mainz Group [9] and also ETMC [13]. The discrepancy with reference [14], which uses some of the same configurations but in some cases different smearing and t_{sink} -values, is mostly likely due to excited state contamination. The near physical point in that study is computed on a subset of the statistics (same smearing and t_{sink}) for ensemble IV. For the higher statistics used in our work, g_A is not consistent with the experimental value at this small volume ($Lm_\pi = 2.7$). The extent of finite volume effects at the near physical point will become clearer once we achieve full statistics on the larger volume, ensemble V ($Lm_\pi = 3.5$).

The effect of excited state contributions can also be seen in the results for $\langle x \rangle_{u-d}$. Our values lie significantly below earlier results of QCDSF [15, 16] and ETMC [17]. Such effects have been seen in previous works [7, 8, 9, 10, 11]. The two volumes at $\beta = 5.29$ and $m_\pi \sim 290$ MeV, and similarly at the near physical point, indicate that finite volume effects are not significant for this quantity. Similarly, the pion mass dependence seems to be mild. The remaining discrepancy with the predictions from PDF parameterisations may be due to lattice spacing effects.

The scalar coupling suffers from larger statistical errors than the other quantities considered here. Within the large error, there is no significant dependence on m_π , volume or lattice spacing. Our results are consistent with other recent determinations. A similar picture is found for the tensor charge, although the statistical errors are smaller in this case.

5. Outlook

Control of excited state contributions and simulation at near physical pion masses are first steps towards a precise determination of g_A and $\langle x \rangle_{u-d}$. For g_A , a careful volume extrapolation is needed, while in both cases the continuum limit needs to be studied. We are extending our simulations with this aim.

6. Acknowledgements

This work is supported by the EU ITN STRONGnet and the DFG SFB/TRR 55. Computations were performed on SuperMUC of the Leibniz Computing Center, the Regensburg iDataCool cluster and the SFB/TR55 QPACE supercomputers. The Chroma software suite [18] was used extensively in this work along with the domain decomposition solver implementation of [19].

References

- [1] A. Sternbeck *et al.*, PoS **Lattice2013**, 291 (2013).
- [2] G. S. Bali *et al.*, (2013), arXiv:1311.1718.
- [3] S. Capitani *et al.*, Nucl.Phys. **B593**, 183 (2001), arXiv:hep-lat/0007004.
- [4] M. Göckeler *et al.*, Phys.Rev. **D82**, 114511 (2010), arXiv:1003.5756.
- [5] M. Constantinou *et al.*, Phys.Rev. **D87**, 096019 (2013), arXiv:1303.6776.
- [6] S. Sint and P. Weisz, Nucl.Phys. **B502**, 251 (1997), arXiv:hep-lat/9704001.
- [7] S. Dinter *et al.*, Phys.Lett. **B704**, 89 (2011), arXiv:1108.1076.
- [8] B. J. Owen *et al.*, Phys.Lett. **B723**, 217 (2013), arXiv:1212.4668.
- [9] S. Capitani *et al.*, Phys.Rev. **D86**, 074502 (2012), arXiv:1205.0180.
- [10] J. Green *et al.*, (2012), arXiv:1209.1687.
- [11] T. Bhattacharya, S. D. Cohen, R. Gupta, A. Joseph, and H.-W. Lin, (2013), arXiv:1306.5435.
- [12] S. Syritsyn, PoS **Lattice2013**, 009 (2013).
- [13] ETM Collaboration, C. Alexandrou *et al.*, Phys.Rev. **D83**, 045010 (2011), arXiv:1012.0857.
- [14] R. Horsley *et al.*, (2013), arXiv:1302.2233.
- [15] A. Sternbeck *et al.*, PoS **LATTICE2011**, 177 (2011), arXiv:1203.6579.
- [16] QCDSF/UKQCD Collaboration, D. Pleiter *et al.*, PoS **LATTICE2010**, 153 (2010), arXiv:1101.2326.
- [17] C. Alexandrou *et al.*, Phys.Rev. **D83**, 114513 (2011), arXiv:1104.1600.
- [18] SciDAC, LHPC, UKQCD, R. G. Edwards and B. Joó, Nucl.Phys.Proc.Suppl. **140**, 832 (2005), arXiv:hep-lat/0409003.
- [19] http://luscher.web.cern.ch/luscher/DD_HMC/index.html.